Title

Dimethyl methylphosphonate adsorption and decomposition on MoO2 as studied by ambient pressure x-ray photoelectron spectroscopy and DFT calculations

Journal

Journal of Physics Condensed Matter, 30(13)

ISSN

0953-8984

Authors

Head, Ashley R

Tsyshevsky, Roman

Trotochaud, Lena

et al.

Publication Date

2018-04-04

DOI

10.1088/1361-648x/aab192

Peer reviewed

Dimethyl Methylphosphonate Adsorption and Decomposition on MoO_2 as Studied by Ambient Pressure X-ray Photoelectron Spectroscopy and DFT Calculations

Ashley R. Head,[1,a] Roman Tsyshevsky,[2,a] Lena Trotochaud,[1] Yi Yu,[1,3] Osman Karslıoğlu,[1] Bryan Eichhorn,[3] Maija M. Kuklja,[2] Hendrik Bluhm[1,4]

[1] Chemical Sciences Division and [4] Advanced Light Source, Lawrence Berkeley National Laboratory, Berkeley, California 94720, United States

[2] Materials Science and Engineering Department and [3] Department of Chemistry and Biochemistry, University of Maryland, College Park, Maryland 20742, United States

[a] These authors contributed equally.

E-mail: hbluhm@lbl.gov

Abstract. (200 words)

Organophosphonates range in their toxicity and are used as pesticides, herbicides, and chemical warfare agents (CWAs). Few laboratories are equipped to handle the most toxic molecules, thus simulants are used as a first step in studying adsorption and reactivity on materials. Dimethyl methylphosphonate (DMMP) is one of the most common non-toxic simulants. Benchmarked by combined experimental and theoretical studies of simulants, calculations offer an opportunity to understand how molecular interactions with a surface changes upon using a CWA which can not be investigated in a common laboratory setting. However, most calculations of DMMP and CWAs on surfaces are limited to adsorption studies on clusters of atoms, which may differ markedly from the behavior on bulk solid-state materials with extended surfaces. We have benchmarked our solid-state periodic calculations of DMMP adsorption and reactivity on MoO_2 with ambient pressure X-ray photoelectron spectroscopy studies (APXPS). DMMP is found to interact strongly with polycrystalline MoO_2, a model system for the MoO_x component in the ASZM-TEDA© gas filtration material. Density functional theory modeling of several adsorption and decomposition mechanisms assist the assignment of APXPS peaks. Our results show that DMMP decomposes with all the products remaining on the surface. The rigorous calculations coupled with a direct experimental probe of electronic structure pave a path to reliable and predictive theoretical studies of CWA interaction with surfaces.

Keywords: chemical warfare agent simulant, solid-state periodic calculations, DMMP, organophosphonate

Introduction

Use of chemical warfare agents (CWAs) will unfortunately remain a persistent safety concern in society for the foreseeable future. Different chemicals consisting of a broad range of functional groups are used as CWAs. Among the most toxic of these chemicals are the organophosphonates. Organophosphonate toxicity ranges from benign to deadly, resulting in their use as pesticides, herbicides, and CWAs [1]. In all of these utilizations, there is a need to protect personnel from exposure to these molecules, to accurately detect minute amounts, and to decompose stockpiles. To improve the current detection, protection, and decomposition technologies, a better understanding of the fundamental chemistry of organophosphonates with a range of materials is necessary.

Facilities to conduct experiments to understand how chemical warfare agents interact with materials and surfaces are understandably rare. As a first step, CWA simulants are used, with dimethyl methylphosphonate (DMMP) being one of the most common [1]. The phosphoryl oxygen and methoxy groups give a first approximation to sarin, soman, and VX, pictured in Figure 1. DMMP lacks a strong, electronegative leaving group, which renders it safe to use yet deficient in mimicking all aspects of the electronic structure of the more toxic molecules. Density functional theory (DFT) calculations afford an opportunity to close the knowledge gap between simulants and live agents; additionally, dependably accurate calculations will reduce the number of experiments with live agents. However, before modeling reactions of real CWAs, the ability of DFT methods to reliably predict decomposition mechanisms of organophosphonates on surfaces needs to be verified. Joint experimental and theoretical studies of surface-facilitated degradation of CWA simulant compounds should, therefore, benchmark DFT performance for modeling and also provide valuable insight in reaction mechanisms.

Due to its relative structural simplicity and decreased toxicity, the chemistry of DMMP on some metal oxides [2–8] has been studied. Results of these experimental studies suggest that DMMP initially adsorbs at Lewis acid sites or surface hydroxyls via its phosphoryl (P=O) oxygen. Subsequent surface-facilitated decomposition of DMMP usually leads to formation of gas-phase methanol, gas-phase

dimethyl ether, and surface-bound methoxy groups through breaking of one of the P-OCH_3 bonds. Two main mechanisms, so called electrophilic and nucleophilic attacks, have been proposed for P-OCH_3 bond breaking. Both of these mechanisms involve formation of a reaction intermediate with a penta-coordinated phosphorus atom and the interaction between DMMP and surface hydroxyl groups. The results of recent DFT modeling suggest that hydrolysis of a P-OCH_3 bond through nucleophilic addition of a surface OH group dominates DMMP decomposition on zirconium hydroxide [9] and zirconium-based metal organic frameworks [10]. However, there is very little known on decomposition of CWA simulants on pristine oxide surfaces and the effect of surface morphology on reactivity of these compounds. In our recent study [11], we proposed mechanisms for the fragmentation of DMMP on copper (II) oxide that are based on results of ambient pressure X-ray photoelectron spectroscopy (APXPS) measurements supported by diffuse reflectance infrared Fourier transform spectroscopy (DRIFTS) experiments and DFT modeling. The proposed mechanisms and structures describe well the changes in the electronic properties and vibrational frequencies observed in APXPS and DRIFTS results. However, we were not able to obtain activation barriers for the main reactions steps due to the complexity of the system.

In a further step towards predictive calculations of CWAs on surfaces, we here report results of joint APXPS and DFT studies of adsorption and decomposition of DMMP on polycrystalline MoO_2, a model for the MoO_x component in ASZM-TEDA© gas filtration materials [12]. Beginning with the adsorption of DMMP on polycrystalline MoO_2, APXPS measurements at pressures up to 10 mTorr of DMMP were analyzed. This technique allows for the collection of chemical state and semi-quantitative elemental information under pressures closer to those used in under realistic operating conditions. Here, the pressure of DMMP in the experiment was about 10% of its equilibrium vapor pressure at room temperature. Results of DFT modeling were then used to study adsorption and fragmentation of DMMP on MoO_2 and provide energies of reactions, activation barriers and relative shifts in the core level binding energies, thus aiding the interpretation of the APXPS data. In the following we will provide a detailed

description of the decomposition of DMMP - as a example for organophsphorus compounds - on oxide surfaces performed using advanced APXPS measurements coupled with state-of-the-art solid state periodic calculations. The good qualitative agreement between experiment and theory affords detailed insights into the mechanisms of DMMP decomposition on MoO_2 and provides the necessary foundation for a future theoretical study of sarin interactions with MoO_2.

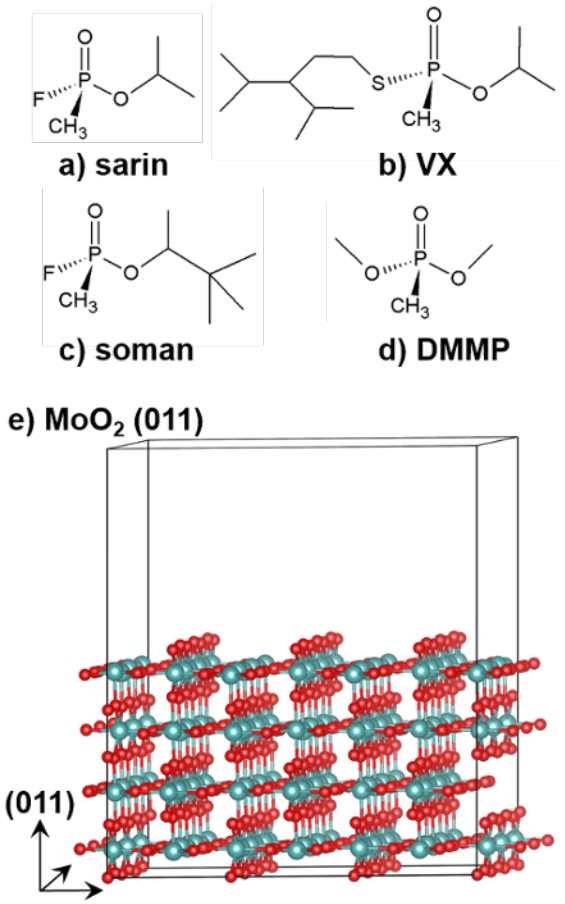

Figure 1. Structures of chemical warfare agents (a) sarin, (b) VX, (c) soman. (d) Structure of the chemical warfare agent simulant dimethyl methylphosphonate (DMMP) and (e) model of a MoO_2 (011) surface used in the simulations of DMMP absorption and decomposition.

Experimental

Ambient Pressure XPS

The experiments were conducted using the APXPS-1 end station [13] at beamline 11.0.2 [14] at the Advanced Light Source at Lawrence Berkeley National Laboratory in Berkeley, CA. The end station is equipped with preparation and analysis chambers, where the base pressures were below 5 x 10^{-9} Torr. A 0.2 mm aperture in the analysis chamber leads to the differentially-pumped electrostatic lens system [15] of the ambient pressure photoelectron spectrometer, allowing for pressures in excess of 1 Torr at the sample surface while collecting XPS data.

A Mo foil (Alpha Aesar, 99.95%) was cleaned in the preparation chamber via sputtering (1 × 10^{-5} Torr Ar^+, 5 mA, 1.5 keV, 15 min) and annealing (900 ºC, 15 min). To prepare the MoO_2 film, the Mo foil was heated to 550 ºC in 1 × 10^{-4} Torr oxygen while monitoring the Mo oxidation state with XPS. The sample was subsequently cooled in vacuum. The dimethyl methylphosphonate (Fluka, >97%) was degassed via freeze-pump-thaw cycles and introduced into the analysis chamber with a precision leak valve. While dosing DMMP, the MoO_2 sample was kept at room temperature (20 °C).

To probe the same sample depth and have the same analyzer transmission function and gas phase scattering for all core levels, photoelectrons of 200 eV kinetic energy were collected by using the following photon energies: 340 eV for P 2p, 435 eV for Mo 3d, 490 eV for C 1s and 735 eV for O 1s. The binding energy was calibrated to the Fermi level of the sample. A Shirley background was subtracted from the O 1s and Mo 3d spectra, and a polynomial background was removed from the P 2p and C 1s spectra. The spectra were fit with Voigt functions. For the P 2p spectra a doublet of Voigt functions with a separation of 0.85 eV [16] and Lorentzian width of 0.03 eV were used. The Lorentzian width of the C 1s spectra was 0.20 eV. Spectra of all core levels at all pressures measured are included in the Supporting Information, including the fit parameters. Binding energies and peak widths were kept constant when fitting the spectra at different pressures. Details of the O 1s fits and corresponding DMMP coverage

calculations are giving in the Supporting Information. All reported binding energies have an estimated error of ± 0.1 eV.

Calculations

Solid-state periodic calculations were performed with density functional theory (DFT) [17,18] using the GGA PBE [19] functional and projector augmented-wave (PAW) pseudo-potentials [20], as implemented in the VASP code [21–23]. In simulating an ideal bulk MoO_2 crystal, a 8×8×8 Monkhorst−Pack k-point mesh and a kinetic energy cut-off of 450 eV were used. Atomic coordinates and lattice constants were allowed to relax simultaneously without any symmetry constraints. The convergence criterion for electronic steps was set to 10^{-5} eV, and the maximum force acting on each atom was set not to exceed 0.02 eV $Å^{-1}$. The calculated lattice parameters of the MoO_2 monoclinic unit cell with $P2_1/c$ space group, $\boldsymbol{a}$ = 5.61 Å, $\boldsymbol{b}$ = 4.91 Å and $\boldsymbol{c}$ = 5.68 Å, agree with the experimental lattice [24] vectors $\boldsymbol{a}$ = 5.61 Å, $\boldsymbol{b}$ = 4.85 Å and $\boldsymbol{c}$ = 5.63 Å within ~1 %.

In the MoO_2 surface calculations (Figure 1c), the model surface slab containing 432 atoms was cut out of the bulk MoO_2 structure to form the (110) surface, with the supercell lattice vectors of a = 22.31 Å, b = 16.82 Å, and c = 33.52 Å. A vacuum layer of 20 Å placed on top of the MoO_2 (011) surface served to minimize interactions between the supercells in the z-direction and to avoid any significant overlap between wave functions of periodically translated cells. All surface calculations were performed at G-point only with a kinetic energy cut-off of 450 eV. The convergence criterion for electronic steps was set to 10^{-5} eV, and the maximum force acting on atoms was set not to exceed 0.03 eV $Å^{-1}$. Minimal energy paths in the VASP periodic calculations were obtained with the nudged elastic band method [25] with five intermediate images. Atomic positions were relaxed using conjugate gradient and quasi-Newtonian methods within a force tolerance of 0.05 Å eV^{-1}. The Kohn-Sham eigenvalues of the core states [26] were used to calculate binding energy shifts collected in Table 1.

Results

Ambient Pressure XPS Experiments

APXPS data were collected while dosing DMMP on a polycrystalline MoO_2 film. First, the polycrystalline MoO_2, which was prepared by oxidizing a Mo foil, was characterized as is. The sharper pair of peaks in the Mo 3d spectrum (Figure 2a) are the $3d_{5/2}$ and $3d_{3/2}$ peaks, with energies matching those in literature [27]. The broader features are satellites from unscreened final states and have a slightly different profile than previously reported spectra [27], likely due to different preparation procedures. The O 1s binding energy (530.1 eV) is consistent with previous reports [27]. A prominent satellite feature likewise occurs in the O 1s spectrum. Unfortunately, this satellite is coincident with binding energies common for hydroxyl groups and molecular water adsorbed on metal oxides [28], making it difficult to evaluate the quantity and effects of these species.

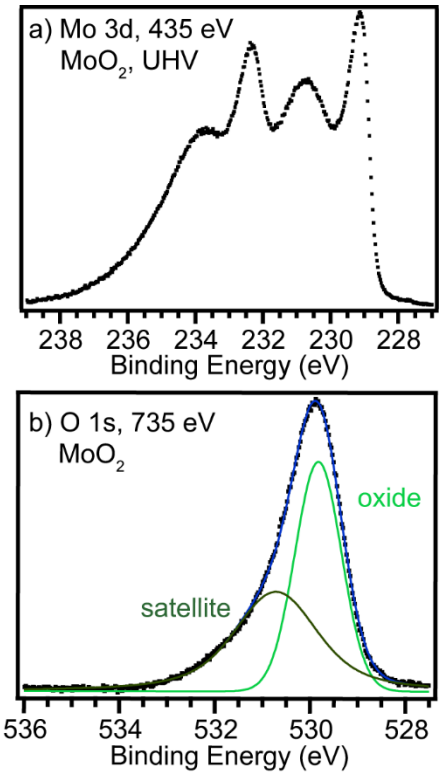

Figure 2. The (a) Mo 3d and (b) O 1s spectra of polycrystalline MoO_2 under UHV conditions match literature spectra. Both core levels have high-binding energy satellites. The black dots are the data points, and the blue line is the sum of the fitted Voigt functions (green).

After the characterization of the clean MoO_2 sample, DMMP was gradually dosed at room temperature into the analysis chamber at order-of-magnitude intervals from 1×10^{-7} Torr to 0.01 Torr. Figure 3 shows a representative P 2p spectrum of the MoO_2 surface at a DMMP pressure of 1×10^{-4} Torr; at this pressure, there is a strong P signal, yet no gas phase DMMP contribution is present, which is often seen at pressures of ~0.01 Torr and above . The main P component has small shoulders on both the high- and low-binding energy sides of the main peak. If the Voigt functions are constrained to a Lorenztian component equal to the natural linewidth of the P 2p ionization (0.03 eV) [29], three sets of doublets are needed to correctly fit the profile. The main peak is assigned to intact, adsorbed DMMP with a P $2p_{3/2}$ binding energy of 133.7 eV. The high binding energy (HBE) component with a peak area of ~10% of the total P has a binding energy of 135.0 eV. The low binding energy (LBE) shoulder at 132.6 eV is ~5% of the total P area. The relative amount of each species does not change significantly over the range of DMMP pressures studied (see Figure S3 and Table S1). These smaller peaks correspond to decomposition products assigned based on DFT calculations, as described below.

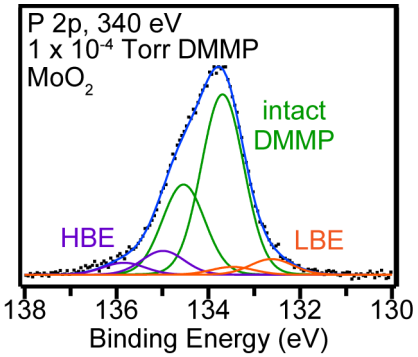

Figure 3. The P 2p spectrum of a MoO_2 film under a DMMP pressure of 1×10^{-4} Torr shows intact DMMP (green) and decomposition products at low (LBE, orange) and high (HBE, purple)

binding energies. The black dots are the data points, and the blue line is the sum of the fitted Voigt doublets.

The C 1s spectrum of MoO_2 at a 1×10^{-4} Torr DMMP (Figure 4) contains two main peaks: the CH_3 signal at 284.8 eV and the OCH_3 signal at 286.6 eV. Analogous to the P 2p spectra, small shoulders arise at the LBE and HBE sides of the main peaks. The assignment of the shoulders will be addressed in conjunction with the DFT calculations. Figure 5 shows the relative amounts of all C species on MoO_2 at all DMMP pressures measured. The relative amount of methyl groups agrees well with the expected amount of 0.33 from the intact DMMP molecule, while the fraction of methoxy groups falls short of the expected 0.67 for molecular adsorption. However, the amount of methoxy, HBE, and LBE carbon species add up to 0.67, indicating that the decomposition products likely result from a reaction of the $POCH_3$ group. The total amount of C expected from the P 2p spectra can be calculated with gas phase sensitivity factors, as further detailed in the Supporting Information. A ratio of the total measured C to the expected C is reported by the orange data points in Figure 5. Values close to 1 suggest that the majority of the carbon-containing decomposition products remain on the surface.

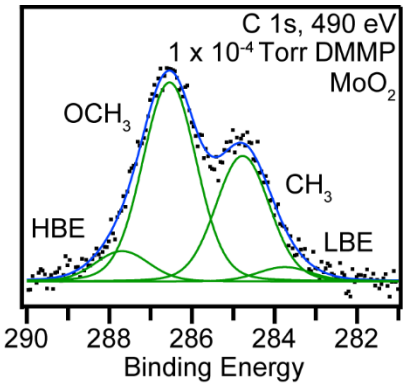

Figure 4. The C 1s spectrum of a MoO_2 film under a pressure of 1×10^{-4} Torr DMMP shows high- (HBE) and low-binding energy (LBE) decomposition products in addition to the expected

methyl (284.8 eV) and methoxy (286.6 eV) groups. The black dots are the data points, and the blue line is the sum of the fitted Voigt functions (green).

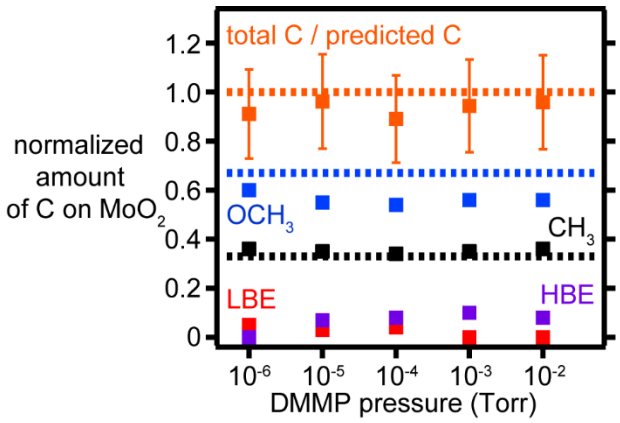

Figure 5. The relative amount of CH_3 (black) matches the amount expected for intact adsorption (black dotted line at 0.33) while the amount of OCH_3 falls short of expected 0.67 (blue). The relative amounts of high- (HBE, purple) and low-binding energy (LBE, red) carbon are also shown. The ratio of the total measured C and the expected C calculated from the P 2p spectra is near 1 at all pressures (orange data points), suggesting decomposition products remain on the surface. The error bars result from the error in the gas phase sensitivity values used in calculated the expected C.

There are no significant changes in the spectral contributions of the substrate upon exposure to DMMP. The Mo 3d satellite intensity decreases slightly upon initial DMMP adsorption and is independent of the DMMP pressure (Figure S5). In addition, no obvious Mo oxidation or reduction upon DMMP adsorption occurs. Likewise, there are no changes to the bulk oxide O 1s peak, shown in Figure 6. The O 1s satellite feature of the bulk oxide peak at 531 eV makes it difficult to extract information about the overlapping P=O signal. The fit in Figure 6 assumed no change in the O 1s satellite parameters after DMMP adsorption. The methoxy peak is clearly identified and used to calculate surface coverages (Figure 7), with the assumption that methoxy groups do not desorb (details are in the Supporting Information). The adsorption affinity, represented by the surface coverage of DMMP on MoO_2, is

compared to that of MoO_3 from our previous work [30], see Figure 7. While the total adsorption of DMMP on pristine is MoO_3 is much lower than that on MoO_2, the presence of hydroxyl groups and oxygen vacancies (OH-MoO_3) strongly increases the coverage on to a level comparable to that on MoO_2.

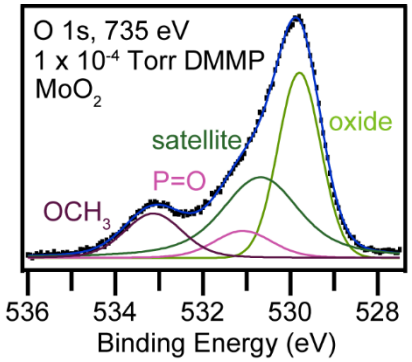

Figure 6. O 1s spectra of DMMP adsorbed onto MoO_2. The black dots are the measured data points, and the blue line is the sum of the fitted Voigt functions representing the oxide substrate (green) and the P=O and OCH_3 groups of DMMP (purple).

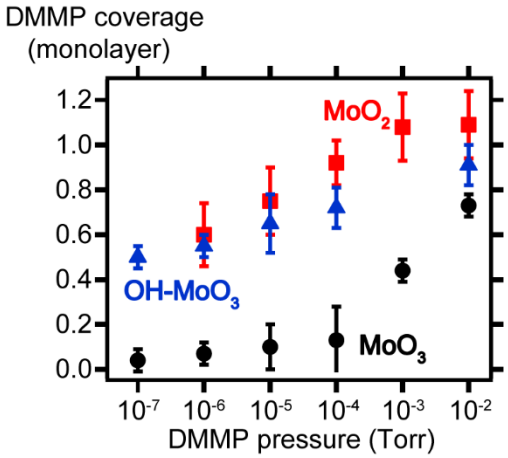

Figure 7. The surface coverages of MoO_2 (red squares) show a stronger interaction with DMMP than MoO_3 (black circles). Adding oxygen vacancies and OH groups to the MoO_3 (OH-MoO_3, blue triangles) brings the coverage closer to that of MoO_2. Error bars result from error in the spectral fits.

Calculations of DMMP Adsorption

DFT calculations of DMMP adsorption and decomposition were conducted to complement and help interpret the APXPS studies. We found that when adsorbed on the MoO_2 (011) surface, DMMP forms a bond with one of the under-coordinated Mo atoms through its phosphoryl oxygen (Figure 8a). This bonding scheme agrees well with the results of DMMP adsorption on other metal oxide surfaces [3,4,31,32]. The calculated adsorption energy (E_{ad}) of -212.7 kJ mol^{-1} points toward a strong chemical bond between the molecule and the surface. For comparison, the calculated E_{ad} values of DMMP on an oxygen-terminated MoO_3 (010) surface with and without an oxygen vacancy are -153.6 kJ mol^{-1} and -96.7 kJ mol^{-1}, respectively [30]. The strength of the interaction is also indicated by the lengthening of the P-O1 bond distance by 0.034 Å between the isolated molecule (1.481 Å) and the DMMP adsorbed on MoO_2 (1.515 Å), a result of the electron density redistribution from the P-O bond towards the O-Mo bond (2.119 Å).

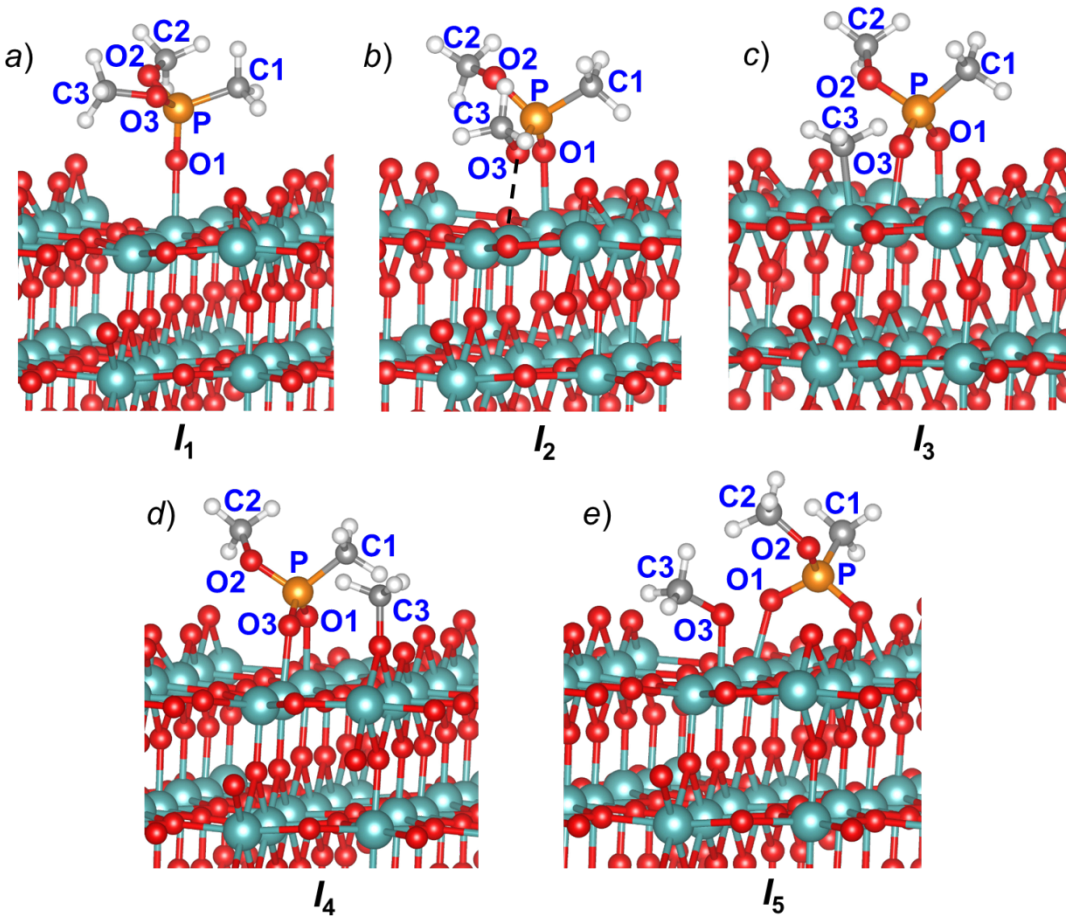

Figure 8. (a) The most favorable adsorption configuration of DMMP adsorbed on MoO_2 (011); (b) intermediate and (c)-(e) final structures involved in DMMP degradation on MoO_2 (011) surface

Calculations of DMMP Decomposition

Our DFT modeling revealed several plausible channels for DMMP degradation on a MoO_2 (011) surface. Initial, intermediate, and final structures involved in the surface-enhanced decomposition of DMMP are shown in Figure 8, with the schematic potential energy diagram depicted in Figure 9. Surface-facilitated decomposition of DMMP begins with rotation of one of the $–OCH_3$ groups about a P-OCH_3 bond (path $\boldsymbol{I_1}$- $\boldsymbol{I_2}$). The calculated activation barrier of such an internal rotation is low and requires only 5.6 kJ mol^{-1}, which is ~15 kJ mol^{-1} lower than in the gas phase [16]. The bond distances P-O3 (1.633 Å)

and O3-C3 (1.472 Å) in the structure $\boldsymbol{I_2}$ (Figure 8b) are elongated by 0.056 Å and 0.01 Å, respectively, as compared to the structure $\boldsymbol{I_1}$ (Figure 8a), suggesting that further decomposition of DMMP will proceed through the cleavage of one of these bonds.

We now discuss three plausible decomposition channels of conformer $\boldsymbol{I_2}$. The first channel proceeds through cleavage of an O-CH_3 bond and adsorption of the methyl group on a surface Mo atom (path $\boldsymbol{I_2}$- $\boldsymbol{I_3}$). The calculated activation barrier of this reaction step is 131.9 kJ mol^{-1}, with the product, structure $\boldsymbol{I_3}$, energetically favored by 80.4 kJ mol^{-1} over structure $\boldsymbol{I_2}$. An alternate outcome of cleaving the O-CH_3 bond is the formation of a surface methoxy group on a terminal oxygen (path $\boldsymbol{I_2}$-$\boldsymbol{I_4}$); this step is more thermodynamically favorable by 36.7 kJ mol^{-1} than the aforementioned formation of a surface Mo-CH_3 moiety (path $\boldsymbol{I_2}$- $\boldsymbol{I_3}$) and requires an activation energy of 131.5 kJ mol^{-1}. Additionally, the barrier for the migration of a methyl group from a Mo atom in $\boldsymbol{I_3}$ to a terminal oxygen atom in $\boldsymbol{I_4}$ is 126.4 kJ mol^{-1}, suggesting that the Mo-CH_3 moiety is short-lived. For comparison, homolytic scission of O-CH_3 bond in the gas phase molecule and the molecule adsorbed on a pristine MoO_3 surface requires significantly higher energies of 344.3 kJ mol^{-1} and 359 kJ mol^{-1}, respectively. Finally, the third plausible channel (path $\boldsymbol{I_2}$-$\boldsymbol{I_5}$) results in a surface methoxy group through cleavage of the P-OCH_3 bond in DMMP and subsequent adsorption of the –OCH_3 moiety on a Mo atom. This pathway results in an energetically favorable product (-66.2 kJ mol^{-1} compared to $\boldsymbol{I_2}$) and the largest activation barrier (149.2 kJ mol^{-1}). Either path of P-OCH_3 bond breaking on the MoO_2 (011) surface is favored by ~240-280 kJ mol^{-1} over that in the isolated gas phase molecule or on pristine as well as reduced MoO_3 (010) surfaces [30].

The results of our DFT modeling suggest that after adsorption onto MoO_2(011) through the phosphoryl oxygen, the O-CH_3 bond of DMMP breaks to form surface methoxy groups as the main products. The most energetically favorable pathway (132.6 kJ mol^{-1}) is $\boldsymbol{I_1}$- $\boldsymbol{I_2}$- $\boldsymbol{I_4}$, where the activation barrier of the rate limiting step $\boldsymbol{I_2}$- $\boldsymbol{I_4}$ is 131.5 kJ mol^{-1}. The alternative channel of forming a Mo-CH_3 intermediate followed by diffusion of the methyl group to a terminal oxygen (pathway $\boldsymbol{I_1}$- $\boldsymbol{I_2}$- $\boldsymbol{I_3}$- $\boldsymbol{I_4}$) requires nearly the same amount of energy as the path $\boldsymbol{I_1}$- $\boldsymbol{I_2}$- $\boldsymbol{I_4}$. We found that on the relatively inert MoO_3 [30], oxygen vacancies and hydroxyl groups improve adsorption of DMMP and trigger its

decomposition. On the other hand, the chemically reactive MoO_2 (011) surface, even in its pristine state, tends to strongly adsorb DMMP and facilitate its further degradation through cleavage of the O-CH_3 bond, without the requirement of surface OH groups or defects. Since the APXPS measurements cannot quantify the hydroxyl groups on this surface due to the O 1s satellite, the effect of hydroxyl groups on DMMP adsorption were not considered in the DFT calculations.

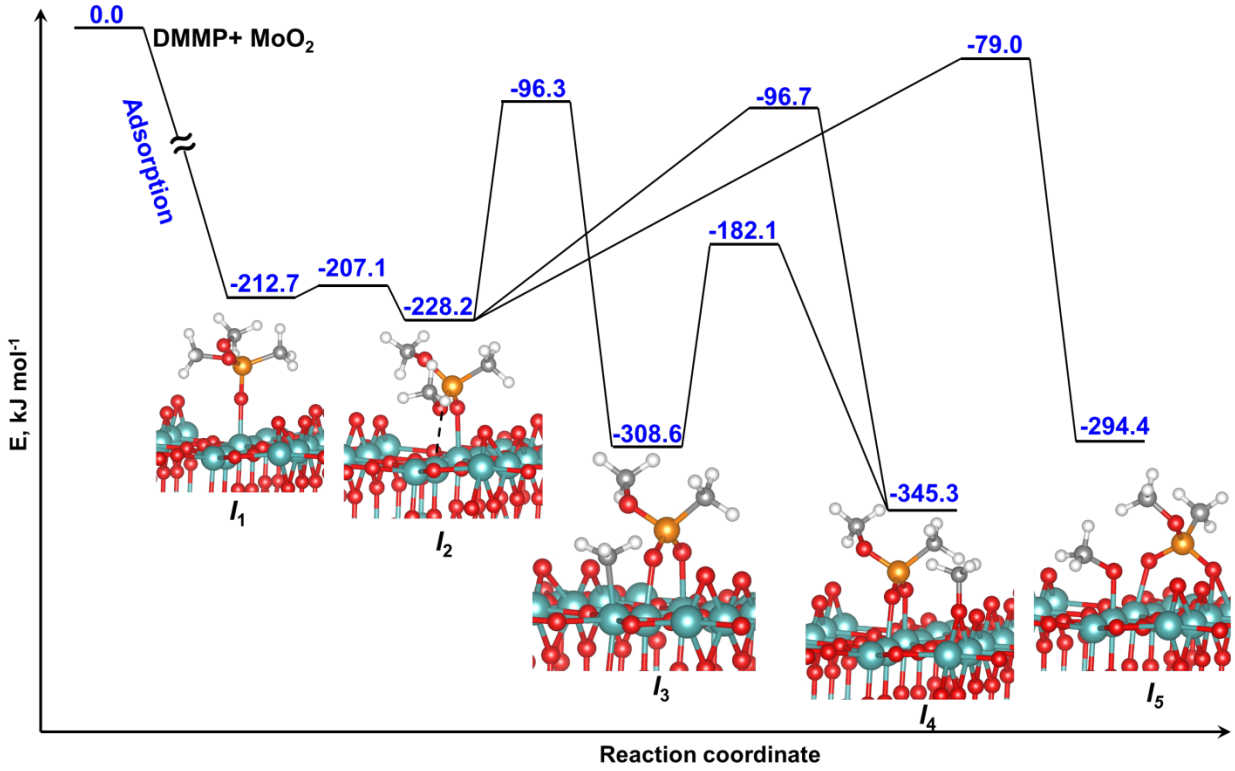

Figure 9. Schematic representation of the potential energy surface associated with the decomposition of DMMP on a pristine MoO_2 (011) surface.

Calculated core level binding energies

To compare the results of DFT simulations with XPS measurements, we calculated core level binding energies for structures involved in the DMMP decomposition on the pristine MoO_2 (011) surface (Figures 8 and 9). The core levels listed in Table 1 show that the rearrangement of the initial adsorption (***I*** $_1$) to ***I*** $_2$ results in relatively small binding energy changes in the majority of the atoms; the exceptions are

the binding energies of the O3 and C3 atoms in the methoxy group directly interacting with the surface, which increase by 0.95 eV and 0.75 eV, respectively. As a result of Mo-OCH_3 formation in configuration $\boldsymbol{I_3}$, significant shifts occur in the 1s core levels of the O3 (-1.40 eV) and C3 (-2.72 eV) atoms. In configuration $\boldsymbol{I_4}$, the methyl group containing the C3 atom is detached from DMMP and adsorbed onto one of the surface oxygen atoms; as a result, the shifts in the core level binding energies of the DMMP residue are very close to those of configuration $\boldsymbol{I_3}$, with the exception of the C3 atom that shifts less. One of the P-OCH_3 bonds is broken to form a methoxy group on the surface through a bond between O3 and a surface Mo atom in configuration $\boldsymbol{I_5}$, resulting in a O3 core level shift of -1.08 eV. Interestingly, the P 2p binding energy in configuration $\boldsymbol{I_5}$ does not significantly shift, despite replacing a methoxy group with a bond to a terminal O atom on the surface. As will be discussed, these calculated core levels are essential in assigning peaks in the APXPS data.

Table 1. Shifts in core level ionization energies (eV) relative to structure $\boldsymbol{I_1}$. The atom labels refer to Figure 8.

Atom	**Core level**	**on (011) MoO_2 surface**				
		$\boldsymbol{I_1}$	$\boldsymbol{I_2}$	$\boldsymbol{I_3}$	$\boldsymbol{I_4}$	$\boldsymbol{I_5}$
O1	**1*s***	0.00	0.33	-0.21	-0.23	-0.15
O2	**1*s***	0.00	0.31	-0.51	-0.48	-0.22
O3	**1*s***	0.00	0.95	-1.40	-1.32	-1.08
P	**2*p***	0.00	0.49	-0.58	-0.54	-0.17
C1	**1*s***	0.00	0.32	-0.33	-0.25	0.03
C2	**1*s***	0.00	0.17	-0.27	-0.26	0.06
C3	**1*s***	0.00	0.75	-2.72	-0.18	-0.01

Discussion

APXPS offers the opportunity to study DMMP adsorption on model surfaces under pressures relevant to applications and provides a benchmark for calculations. Of great importance to applications is the quantification of the adsorption of molecules on materials as a function of partial pressure. ASZM-TEDA© filtrers contain MoO_x, and thus a comparison of DMMP adsorption on MoO_2 and MoO_3 is of

direct interest to the understanding of the chemistry of this material. Figure 7 shows that DMMP interacts more strongly with MoO_2 than MoO_3 due to the under-coordinated Mo atoms inherent in the MoO_2 structure. In contrast, the thermodynamically stable MoO_3 (010) surface is oxygen terminated, resulting in only a weak interaction with DMMP [30,33], but the surface coverage can be increased to the level of MoO_2 by adding favorable binding sites, including surface OH groups and oxygen vacancies [30]. Surface coverages offer an initial empirical step with which to correlate DFT calculations. The stronger interaction with MoO_2 is echoed in the calculated E_{ad} that is about 100 kJ mol^{-1} more favorable than that of MoO_3 [30].

DFT calculations are further used to aid in the interpretation of the XPS data. The APXPS spectra provide information on the presence of reaction products, but only indirect information on reaction mechanisms. By predicting decomposition pathways in DFT, likely products can be identified and correlated with the XPS data. The calculated core level shifts of the predicted surface species are presented in Table 1 and have been used to identify the decomposition products in the P 2p and C 1s spectra. In Figure 3, the main peak in the P 2p spectrum is assigned to intact adsorption (structure ***I*$_1$**), and the core level shifts in Table 1 are referenced to the binding energies in this structure. Differences in the quantitative agreement between calculated and measured shifts are due to many factors. For example, the calculations were limited to a pristine, idealized MoO_2 (011) surface, which is the most stable surface of MoO_2, whereas XPS measurements were measured on polycrystalline samples with different surface facets and concentrations of defects. Thus, assignment of the experimental peaks was based on qualitative comparison with calculated data. The DFT calculations forecast that only structure ***I*$_2$** (Figures 9 and 11) should have a larger P 2p signal, though the predicted +0.49 eV shift is only one-third of the actual shift of the HBE P 2p peak. The binding energy of the HBE C 1s peak in Figure 4a also suggests structure ***I*$_2$**, with the predicted shift of +0.75 eV close to the +1.2 eV shift from the spectra. The similar amount of HBE P 2p and C 1s areas (~10%, cf. Tables S1 and S2) at all DMMP pressures lend further support for assigning these peaks together to structure ***I*$_2$**. A peak from the O3 atom of ***I*$_2$** at +0.95 eV higher than the

intact methoxy signal is lacking from the O 1s spectrum; however, using the gas phase sensitivity factors to approximate the O 1s signal for ***I₂*** (see Supporting Information), only a few percent of the total O 1s signal would be expected for this peak. Therefore, it is reasonable that such a peak is not resolvable in the O 1s spectrum.

In regards to the LBE C 1s and P 2p components in the spectra of DMMP adsorbed onto MoO_2, structure ***I₃*** initially appears a strong candidate for assignment. The P has a calculated shift of -0.58 eV that is half of the experimentally seen -1.1 eV shift in Figure 3. However, the -2.72 eV shift of the Mo-CH_3 moiety (C3) is significantly larger than the experimental -1.0 eV shift (Figure 4a). While this calculated shift agrees with previous assignments of Mo-C metal bonds that are expected around 282.7 eV (for molybdenum carbide [34] and CO adsorbed on Mo metal [35]) it is too large to assign the LBE C 1s peak in Figure 4a to a Mo-CH_3 group. Furthermore the calculations indicate that structure ***I₃*** is likely a short-lived intermediate as the activation barrier for the CH_3 group to migrate from a Mo atom to a terminal O atom is quite low.

Structure ***I₄*** is likely responsible for the LBE peaks in the C 1s and P 2p spectra, as indicated by the decrease in the core level binding energy in Table 1. The predicted core level shifts for ***I₅*** are quite small and not detectable in our XPS measurements. The activation barrier to generate ***I₅*** is the highest among all structures considered here, yet still accessible under operational conditions. Consequently, we can neither confirm nor disregard ***I₅*** since the peaks from this species would overlap with the signal from other configurations.

The P 2p data show that about 15% of the total adsorbed DMMP decomposes on the MoO_2 (011) surface. Due to the inherently larger availability of coordination sites on MoO_2, adsorption and decomposition there is more extensive than on MoO_3. The effect of OH groups and oxygen vacancies on MoO_2 could not be probed here due to the O 1s satellite peak. In our previous study of MoO_3, we found that introducing oxygen vacancies and hydroxyl groups increased DMMP coverage, and hydroxyl groups

are necessary for the formation of volatile methanol. In the case of MoO_2, the amount of C on the surface matches the predicted amount calculated from the P spectrum, indicating minimal methanol desorption.

While our polycrystalline samples most likely showed a distribution of surface terminations, the MoO_2 (011) surface is the most thermodynamically stable, and the calculations of DMMP adsorption on this surface are consistent with our experimental results. The MoO_2 (011) surface can be described as distorted rutile, and it is thus of interest to compare its surface chemistry to that of rutile TiO_2 (110). Zhou et al. studied DMMP adsorption on TiO_2 (110) under UHV conditions [36] and found DMMP decomposition at room temperature decomposition on reduced TiO_2 (110)-(1 × 2) [37], while DMMP was found to adsorb in its intact form on the stoichiometric TiO_2 (110) (1×1) surface [37]. This is in agreement with our results that show that the majority of DMMP adsorbs intact on MoO_2. While we have explored decomposition pathways on a pristine MoO_2 surface using DFT (which suggest decomposition without the need of surface OH and/or defects), we cannot exclude that the variety of crystal facets present in our polycrystalline samples contribute to the decomposition, in a similar fashion to the reduced Ti sites in the reconstruction of TiO_2 [36,37]. There have been several infrared spectroscopy studies of powdered TiO_2 with nanoparticles containing 70% anatase and 30% rutile [3,5,38,39]. In general at room temperature, hydroxyl groups are the initial interaction sites with the phosphoryl oxygen. Under-coordinated Ti atoms are the next most energetically favorable binding sites. Surface-bound methyl methylphosphate and methoxy groups are the main decomposition products on TiO_2, just as in MoO_2, where reaction with surface hydroxyl groups leads to the formation of methanol. In addition there are two other, less prominent, decomposition pathways: P-CH_3 cleavage and formation of a surface-bound carboxylate intermediate [5]. XPS does not show evidence of P-CH_3 cleavage on MoO_2, and the DFT calculations also indicate that P-CH_3 cleavage is energetically not favored. The HBE C 1s peak in Figure 4a has a binding energy close to that of a carboxylate species. While this species was observed on the surface for only a few minutes in the study of DMMP on TiO_2 [5], it is unlikely it would be observed our XPS

experiments, where equilibrium is allowed to establish and measurements of all elements take ~ 30 minutes at each pressure.

Conclusions

APXPS measurements of polycrystalline MoO_2 exposed to DMMP were used to benchmark DFT calculations of DMMP adsorption and decomposition. Calculated core level shifts aided in the assignment of species in the APXPS data; the predicted decomposition pathways were found to agree with a quantitative analysis of the spectra. After initial molecular adsorption of the phosphoryl oxygen to an under-coordinated Mo atom, surface-bound methoxy groups form through the breaking of a P-OCH_3 bond. No volatile decomposition products form. The under-coordinated metal atoms of MoO_2 permit a stronger interaction with DMMP and different decomposition products compared to MoO_3. The DFT calculations presented here advance the theoretical investigations of the DMMP/metal oxide systems beyond simple surface adsorption towards more complex reactions on surfaces.

Acknowledgements

This work was funded by the Department of Defense through the Defense Threat Reduction Agency (Grant HDTRA11510005). R.T. and M.M.K acknowledge support from NSF XSEDE resources (Grant DMR-130077) and DOE NERSC resources (Contract DE-AC02-05CH11231) and computational resources at the Maryland Advanced Research Computing Center (MARCC). MMK is grateful to the Office of the Director of National Science Foundation for support under the Independent Research and Development program. Any appearance of findings, conclusions, or recommendations expressed in this material are those of the authors and do not necessarily reflect the views of NSF. The Advanced Light Source is supported by the Director, Office of Science, Office of Basic Energy Sciences, of the U.S. Department of Energy under Contract No. DE-AC02-05CH11231.

[1] Jang Y J, Kim K, Tsay O G, Atwood D A and Churchill D G 2015 **115** PR1

[2] Mitchell M B, Sheinker V N and Mintz E A 1997 *J. Phys. Chem. B* **101** 11192

[3] Rusu C N and Yates Jr J T 2000 *J. Phys. Chem. B* **104** 12292

[4] Mitchell M B, Sheinker V N, Cox Jr W W, Gatimu E N and Tesfamichael A B 2004 *J. Phys. Chem. B* **108** 1634

[5] Panayotov D A and Morris J R 2009 *Langmuir* **25** 3652

[6] Aurian-Blajeni B and Boucher M M 1989 *Langmuir* **5** 170

[7] Li Y-X, Schlup J R and Klabunde K J 1991 *Langmuir* **7** 1394

[8] Gordon W O, Tissue B M and Morris J R 2007 *J. Phys. Chem. C* **111** 3233

[9] Schweigert I V and Gunlycke D 2017 *J. Phys. Chem. A* **121** 7690

[10] Wang G, Sharp C, Plonka A M, Wang Q, Frenkel A I, Guo W, Hill C, Smith C, Kollar J, Troya D and Morris J R 2017 *J. Phys. Chem. C* **121** 11261

[11] Trotochaud L, Tsyshevsky R, Holdren S, Fears K, Head A R, Yu Y, Karslıoğlu O, Pletincx S, Eichhorn B, Owrutsky J, Long J, Zachariah M, Kuklja M M and Bluhm H 2017 *Chem. Mater.* **29** 7483

[12] Morrison R W 2001 NBC Filter Performance; ECBC-TR-135; U.S. Army Soldier and Biological Chemical Command: Aberdeen Proving Grounds, MD

[13] Ogletree D F, Bluhm H, Hebenstreit E D and Salmeron M 2009 *Nucl. Instrum. Methods Phys. Res., Sect. A.* **601** 151

[14] Bluhm H, Andersson K, Araki T, Benzerara K, Brown G E, Dynes J J, Ghosal S, Gilles M K, Hansen H-Ch, Hemminger J C, et al 2006 *J. Electron Spectrosc. Relat. Phenom.* **150** 86

[15] Ogletree D F, Bluhm H, Lebedev G, Fadley C S, Hussain Z and Salmeron M 2002 *Rev. Sci. Instrum.* **73** 3872

[16] Head A R, Tsyshevsky R, Trotochaud L, Eichhorn B, Kuklja M M and Bluhm H 2016 *J. Phys. Chem. A* **120** 1985

[17] Hohenberg P and Kohn W 1964 *Phys. Rev.* **136** B864

[18] Kohn W and Sham L J 1965 *Phys. Rev.* **140** A1133

[19] Perdew J P, Burke K and Ernzerhof M 1996 *Phys. Rev. Lett.* **77** 3865

[20] Blöchl P E 1994 *Phys. Rev. B* **50** 17953

[21] Kresse G and Furthmüller J 1996 *Comput. Mater. Sci.* **6** 15

[22] Kresse G and Furthmüller J 1996 *Phys. Rev. B* **54** 11169

[23] Kresse G and Hafner J 1993 *Phys. Rev. B* **47** 558

[24] Brandt B G and Skapski A C 1967 *Acta Chem. Scand.* **21** 661

[25] Henkelman G, Uberuaga B P and Jónsson H 2000 *J. Chem. Phys.* **113** 9901

[26] Köhler L and Kresse G 2004 *Phys. Rev. B* **70** 165405_

[27] Scanlon D O, Watson G W, Payne D J, Atkinson G R, Egdell R G and Law D S L 2010 *J. Phys. Chem. C* **114** 4636

[28] Ketteler G, Yamamoto S, Bluhm H, Andersson K, Starr D E, Ogletree D F, Ogasawara H, Nilsson A and Salmeron M 2007 *J. Phys. Chem. C* **111** 8278

[29] Krause M O and Oliver J H 1979 *J. Phys. Chem. Ref. Data* **8** 329

[30] Head A R, Tsyshevsky R, Trotochaud L, Yu Y, Kyhl L, Karslıoğlu O, Kuklja M M and Bluhm H 2016 Adsorption of Dimethyl Methylphosphonate on MoO_3 : The Role of Oxygen Vacancies *J. Phys. Chem. C* **120** 29077–88

[31] Chen D A, Ratliff J S, Hu X, Gordon W O, Senanayake S D and Mullins D R 2010 *Surf. Sci.* **604** 574

[32] Bermudez V M 2007 *J. Phys. Chem. C* **111** 3719

[33] Head A R, Tang X, Hicks Z, Wang L, Bleuel H, Holdren S, Trotochaud L, Yu Y, Kyhl L, Karslıoğlu O, et al. 2017 *Catal. Struct. React.* **3** 112

[34] Ramqvist L, Hamrin K, Johansson G, Fahlman A and Nordling C 1969 J. Phys. Chem. Solids 30 1835

[35] Fryberger T B, Grant J L and Stair P C 1987 Langmuir 3 1015

[36] Zhou J, Varazo K, Reddic J E, Myrick M L and Chen D A 2003 Anal. Chim. Acta 496 289

[37] Zhou J, Ma S, Kang Y C and Chen D A 2004 J. Phys. Chem. B 108 11633

[38] Moss J A, Szczepankiewicz S H, Park E and Hoffmann M R 2005 J. Phys. Chem. B 109 19779

[39] Panayotov D A and Morris J R 2009 J. Phys. Chem. C 113 15684